# A Modified Surface Forces Apparatus for Single Molecule Tracking

**Arne Schob and Frank Cichos***

*Photonics and Optical Materials, Institute of Physics, Chemnitz University of Technology, 09107 Chemnitz, Germany*

*Received: September 14, 2005; In Final Form: January 12, 2006*

To unravel molecular motion within confined liquids, we have combined a surface forces apparatus (SFA) with a highly sensitive fluorescence microscope. Details of our setup including important modifactions to enable the tracking of single dye molecules within nanometer thin confined liquid films are presented. The mechanical and optical performance of our setup is discussed in detail. For a load of 20 mN we observed a circular-shaped contact region ($d \approx 300$ $\mu$m), which results in a confining pressure of about 280 kPa. First experiments on liquid films of tetrakis(2-ethylhexoxy)silane (TEHOS) doped with rhodamine B demonstrated the ability to track single dye molecules within the confining gap of a SFA. The mean diffusion constant was independent of the liquid film thickness of $\sim 3 \times 10^{-8}$ cm$^2$/s and thus 10 times smaller than the diffusion constant of rhodamine B in bulk TEHOS. This points to the existence of a thin interface layer with slower molecular dynamics and an attractive potential parallel to the solid surface trapping molecules in this interface region.

## 1. Introduction

The surface forces apparatus technique (SFA), first set up almost 30 years ago[1,2] and later modified and improved several times,[3−6] has been used intensively to study interactions at the liquid−solid-interface. Experiments carried out with surface forces apparatuses cover investigations of structural forces,[7] drainage of thin liquid films,[8] phase transitions in confined liquids,[9−11] lubricated friction with stick-slip sliding,[12] friction of polymerbrushes,[13,14] friction in thin alcohol films,[15,16] dynamics of layering transitions,[17] and many other similar topics. All of these experiments are ensemble experiments and therefore restricted to the measurement of mean values of physical properties rather than distributions. Because of this, they are unable to reveal either details of molecular motion within the sample liquid or physical parameters (e.g., diffusion constants, shear induced drift rates, mobility of molecules, duration of attachment periods at the solid−liquid interface) on a single-molecule level. Their ability to resolve spatial heterogeneities within the sample liquid is limited by the probed volume, which is usually more than several $\mu$m$^3$.

Recently, there have been first attempts to access the dynamics in confined liquids on a molecular level by applying fluorescence correlation spectroscopy (FCS) to the confining gap of a SFA.[18,19] While FCS has single-molecule detection sensitivity, it provides a reliable signal only by averaging over a large number of events. Thus, FCS gives only the ensemble-averaged diffusion constant including a mean viscosity for the probed volume. For FCS, this volume is determined by the size of the focal spot of a confocal microscope, which can be as small as about 300 nm in diameter in the focal plane. This allowed for the first time the observation of spatial changes in the contact region of a SFA, but it still prevents the measurement of any physical parameters of a single molecule.

Direct observation and tracking of tracer molecules by single molecule detection is able to provide access to molecular motion in a much more detailed way. The position of each tracer molecule can be determined with an accuracy better than $\Delta x = 50$ nm and with a sufficient temporal resolution (down to 10 ms). This true single-molecule sensitivity may therefore directly reveal distributions of certain physical parameters, whereas the experiments mentioned above deliver the mean of those distributions only. The advantages of single molecule tracking become even clearer once the anistropy of molecular motion is investigated. While single molecule tracking enables the detection of anisotropic motion most directly from single molecule trajectories, it is difficult to obtain from FCS or other ensemble techniques. Therefore, single molecule tracking combined with a SFA opens the way to a huge number of analytical approaches, exceeding the abilities of FCS and other ensemble experiments by orders of magnitude.

Single molecule tracking has already been used in different experiments for a couple of years and was successfully applied to study dynamics in polymers near the glass transition,[20,21] transport processes in biological systems,[22−24] diffusion within molecular sieves,[25,26] diffusion in nonoporous sol−gel networks,[27] molecular dynamics in thin liquid films near solid substrates,[28,29] and many others. To apply the benefits of this technique to confined liquids we will present a combined setup for surface forces measurements with crossed cylinder geometry and simultaneous observation of single dye molecules as tracers for the molecular motion within the sample liquid.

A crucial part of all SFA experiments is the measurement of the liquid's film thickness. This is commonly done optically[30] by silvering the substrates to form an interferometer. However, the need for high detection efficiencies in single molecule tracking makes this approach impracticable. Other ways to measure the surface separation are the use of bimorph cantilevers[31] or direct capacitive observation of the silver layers forming a capacitor.[32,33] We have chosen a slightly different approach and placed a capacitive position sensor[34,35] into the setup some centimeters away from the approaching surfaces. For first single molecule tracking experiments we used tetrakis-(2-ethylhexoxy)silane (TEHOS), a nonpolar liquid with spherical

* To whom correspondence should be addressed. Tel: +49-371-5313066. Fax: +49-371-5313060. E-mail: cichos@physik.tu-chemnitz.de.

10.1021/jp055201+ CCC: $33.50 
Published on Web 02/09/2006

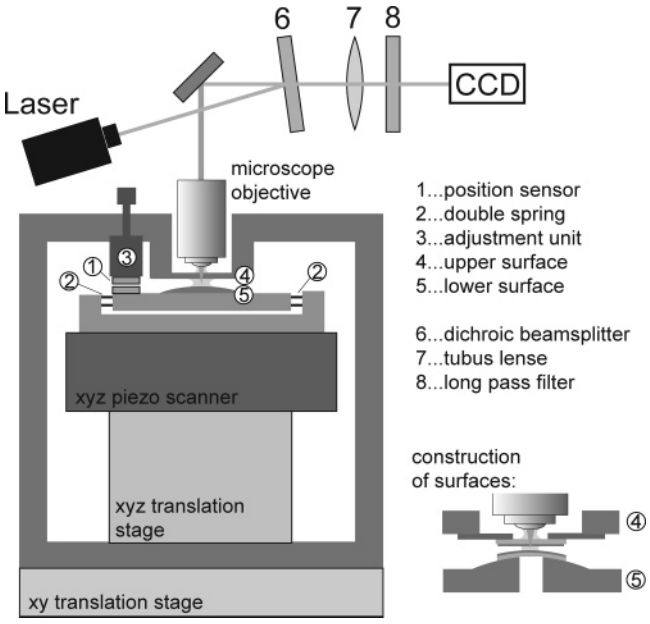


**Figure 1.** Scheme of the combined setup. Details are given in the text. Composition of the cylinder surfaces is shown in detail.

molecules (1 nm diameter), which has been used in spreading experiments.[36] Compared to the frequently used octamethylcyclotetrasiloxane (OMCTS) it has a much lower evaporation rate and a less perfect environmental control is needed. Additionally, TEHOS has a higher bulk viscosity compared to OMCTS, which simplifies single molecule tracking.

## 2. Experimental Section

The combined setup mainly consists of two parts, a home-built highly sensitive wide field fluorescence video microscope and a home-built surface forces apparatus, which can be placed beneath the objective of the microscope (Figure 1). The whole apparatus is mounted on an optical table with air damped feet for vibration insulation and can be put into an enclosure for thermal stability.

The microscopy part of the setup contains an immersion objective (OLYMPUS UPlanApo, 100x, NA 1.35), by which the sample is illuminated with circular polarized light (532 nm) from a frequency doubled Nd:YAG laser (Pusch OptoTech) at 10 mW (0.6 kW/cm$^2$). Single molecule fluorescence is then collected by the same objective and directed onto an on-chip amplified CCD camera (RoperScientific Cascade:512F). Remaining excitation light is separated from luminescence by a dichroic beam splitter (OmegaFilters XF2030 525DRLP) and blocked by a long-pass detection filter (Chroma HQ545LP). The acquisition of image series is done with a fast computer. With image sizes of 100 $\times$ 100 pixels (16 $\times$ 16 $\mu$m) we are able to record more than 1000 frames with exposure times down to 10 ms.

The SFA part of the setup is formed by an aluminum frame, with the upper curved surface rigidly attached to it. The lower surface is mounted into the same frame via a double spring ($k$ = 4.7 kN/m), a closed loop piezo scanner (PI) and a xyz-translation stage (Martok). In this way, the lower surface can be moved by several millimeters in all three dimensions with subnanometer precision. One plate of a capacitive position sensor pair (PI) is mounted to each of the surfaces. The upper sensor plate can be adjusted by micrometer screws (tilt and distance) for optimal operation. The cylinder surfaces are formed by an aluminum frame (radius of curvature 70 mm) on which suprasil slides ($d$ = 100 $\mu$m) are glued directly on top of an observation apperture (diameter 10 mm). On these curved quartz surfaces thin slides of mica (Goodfellow) are mounted by adhesion forces and cleaved afterward according to Frantz and Salmeron[37] with adhesive tape to a final thickness of less than 5 $\mu$m. The whole SFA can be moved horizontally by a *xy*-translation stage (Newport) with respect to the microscope objective. All electronic parts of the SFA are remote controlled by a separate computer.

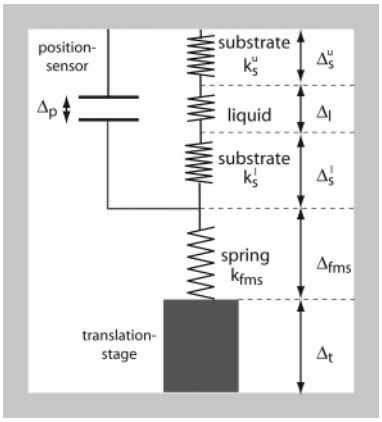


**Figure 2.** Scheme of SFA mechanics. $\Delta_l$, $\Delta_s^l$, $\Delta_s^u$, $\Delta_{fms}$, and $\Delta_t$ denote the change in the liquid film thickness, the change in the deformation of lower and upper substrate, the deflection change of the force measuring spring, and the displacement change of the translation stage, respectively. The change of the signal of the position sensor is denoted by $\Delta_p$, while the elasticities of the force measuring spring and lower and upper substrate are given as the spring constants $k_{fms}$, $k_s^l$, and $k_s^u$, respectively. For simplicity, both substrates will be described together by $\Delta_s = \Delta_s^l + \Delta_s^u$ and $k_s = (1/k_s^l + 1/k_s^u)^{-1}$. The rigidity of the frame ensures $\Delta_l + \Delta_s + \Delta_{fms} + \Delta_t = 0$ and $\Delta_p = \Delta_l + \Delta_s$.

We have chosen rhodamine B (RhB) as tracer dye, because its absorption spectrum fits well the emission of the laser light source. It is dissolved in TEHOS at a concentration of about 5 $\times$ 10$^{-10}$ M and exhibits almost no blinking and bleaching on the time scale of the experiment (20 ms to 20 s).

Mechanical experiments were carried out fully automated during nighttime in a basement laboratory to prevent human induced disturbances. The measurements themselves were started not earlier than several hours after sample preperation and mounting to achieve good thermal equilibrium within the setup.

## 3. Mechanics

Each SFA setup must be able to measure the applied load on the surfaces and the resulting thickness of the sample film simultaneously. We will discuss this process for our experimental setup in more detail to show the origin of performance restrictions we encountered. A scheme with all employed parameters is depicted in Figure 2.

Both tasks, the force and liquid film thickness measurement, are reduced to a measurement of a displacement. To obtain the applied load the deflection of a spring with known spring constant $k_{fms}$ is observed while moving one surface against the other. In this way, changes of the acting force can be calculated as

$$\Delta F = k_{fms}(\Delta_t + \Delta_p) \quad (1)$$

where $\Delta_t$ is the performed movement of the piezo translation stage and $\Delta_p$ the recorded signal change at the position sensor. The accuracy of force change detection $\sigma_F$ is then given by

$$\sigma_F = \sigma_k^{fms}(\Delta_t + \Delta_p) + k_{fms}(\sigma_t + \sigma_p) \quad (2)$$

with $\sigma_k^{fms}$, $\sigma_t$, and $\sigma_p$ being the uncertainties of the force

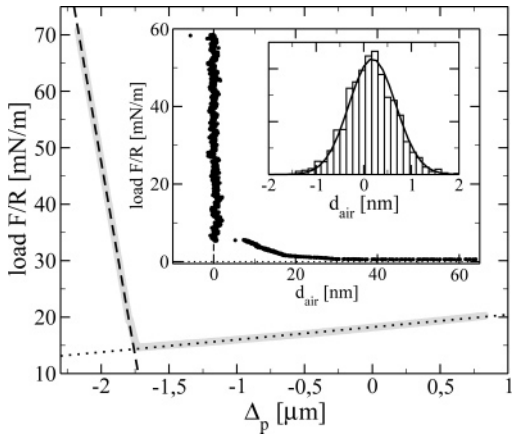


**Figure 3.** Approach of dry crossed cylinder quartz surfaces. The graph shows the recorded raw data (gray) and corresponding linear fits. The load axis is normalized by the radius of curvature of the quartz surfaces. The spring constant of the quartz substrate is $k_s = 9.8$ kN/m (dashed regression), the error of the slope of the regression is $\sigma_k^s = 4 \times 10^{-3}$ kN/m. The dotted regression corrects for a slight linear misalignment of the position sensor. After applying this correction and eq 5, we get the applied load as a function of the real air gap width, as shown in the inset (data were calibrated with $d_{air}(F \rightarrow \infty) \equiv 0$ and $F(d_{air} \rightarrow \infty) \equiv 0$). The second inset shows the distribution of residuals of the linear regression for $F/R > 6$ mN/m. The standard deviation of the residuals is $\sigma = 0.49$ nm. The deviation from a straight line for small loads is attributed to surface roughnesses. The point of contact for ideal surfaces is marked by the intersection of dashed and dotted lines.

measuring spring constant, the piezo translation stage movement and the position sensor signal change, respectively.

If the film thickness of the sample liquid changes because of a changed load, the substrate deformation will change as well, which causes the position sensor signal to change as the sum of both. Because the applied normal force is acting upon sample and substrate in the same way, both will be deformed if the force changes. However, only the deformation of the liquid film shall be determined. Assuming the elasticity of the substrate is known (or can be obtained by a simple calibration measurement), we can detect thickness changes $\Delta_l$ of the liquid film. Usually, the substrates for SFA experiments are made of thick glass lenses and their elasticity is covered by Hertz' theory resulting in a power law for the surface deformation[38]

$$\Delta_s \sim F^{2/3} \tag{3}$$

Our setup uses thin slides of quartz, which correspond much more to deformable membranes as described in text books. Although the applied load is acting via the contact area ($d_{contact} < 0.3$ mm), it can be treated as pointlike, since the membrane is much larger ($d_{membrane} = 10$ mm) than the area of contact. The deformation of a membrane with a pointlike load acting at it's center is given by[39]

$$\Delta_s \sim F \tag{4}$$

In fact, real surfaces will show a combination of both hertzian-like deformation and membrane-like bending with a ratio depending on the experimental geometry. To evaluate this behavior for our surfaces, we measured the deformation $\Delta_s$ as a function of the applied load $F$ without liquid within the confining gap for different types of substrates, pure quartz slides (Figure 3), quartz slides with mica attached by adhesion forces, and quartz slides with glued mica. Only the latter case gave a remarkable deviation from a linear deformation as expected for membranes. For the first two cases, the power law part of the deformation is just a very small correction and will be neglected for further analysis. With that, substrates without glue follow a membrane-like elasticity, which can be covered by a single number, the spring constant $k_s$ of the substrate. We use substrates without a glue layer only, and therefore, we can calculate the liquid film thickness change as

$$\Delta_l = \Delta_p + \frac{\Delta F}{k_s} = \Delta_p + \frac{k_{fms}}{k_s}(\Delta_p + \Delta_t) \tag{5}$$

The accuracy $\sigma_l$ of measuring this film thickness change $\Delta_l$ can then be given as

$$\sigma_l = \sigma_p + (\sigma_p + \sigma_t)\frac{k_{fms}}{k_s} + (\Delta_p + \Delta_t)\left[\frac{\sigma_k^{fms}}{k_s} + \frac{k_{fms}\sigma_k^s}{(k_s)^2}\right] \tag{6}$$

Figure 3 shows the results of a dry approach with pure Suprasil quartz substrates (no liquid film between). Since $\Delta_l$ equals zero for a dry contact of the substrates, eq 5 reduces to $\Delta F/k_s = -\Delta_p$, and $k_s$ can be directly obtained from the slope of the curve in Figure 3 for $\Delta_p < -1.7$ $\mu$m.

## 4. Optics

Observation of single fluorescent dye molecules using a wide-field video microscope has gradually become a standard application during the last couple of years. Most important ingredients to carry out such experiments are a highly sensitive and fast CCD, an excellent objective with high NA, and of course, ultra-clean, nonfluorescent substrates. In particular, the latter two conditions are critical when applying video microscopy to a surface forces apparatus. Further high NA objectives possess a short working distance (a few 100 $\mu$m). Although it is necessary for the curved substrates to withstand high loads, they must be thin enough to enable the optical observation of the confined sample. We solved this problem by gluing bent quartz slides onto a curved aluminum frame with an aperture hole directly beneath the slides. By selecting an immersion objective with appropriate geometry we are able to image the liquid film with NA = 1.35.

Experiments in a SFA require atomically smooth surfaces. Therfore, usually mica is glued onto a glass cylinder and forms the innermost surface. As expected, a sandwich of glass, glue, and mica as a multilayer system produces optical distortions, reflections, and stray light, which drastically reduces the image quality. Additionally, all tested optical glues were highly fluorescent, which prevented the detection of single molecules. Therefore, thin mica sheets were mounted onto the quartz slides just by pure adhesion forces.

To characterize the quality of single molecule measurements, we have determined the achieved signal-to-noise-ratio (SNR), which is directly related to the achievable localization accuracy for single emitters. For experiments (RhB in TEHOS) within the SFA we have achieved SNR = 3, which is much less than on simple substrates (same liquid on a simple quartz slide: SNR = 20), but still good enough to track single molecules. The tracking itself is done by means of imageprocessing with a home-built software package. A first characterization of the observed molecule can be achieved by simply calculating the diffusion coefficient by a weighted fit to the mean squared displacement.[40]

## 5. Results and Discussion

The mechanical long term behavior of the setup was tested by recording the readings of the capacitive position sensor. As can be seen in Figure 4, it took more than 2 days to reach a sufficient thermal equilibrium with small drift rates of about

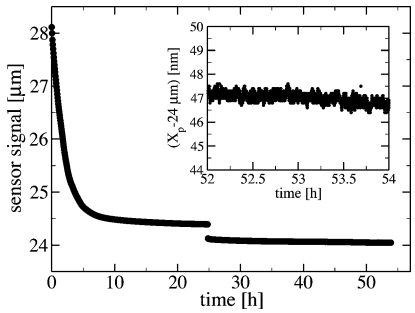


**Figure 4.** Long-term stability of the SFA setup. Displayed are the readings of the position sensor starting directly after installing the whole setup in a new laboratory. Equilibration takes more than 2 days. The final drift rate is less than 0.5 nm/h (inset).

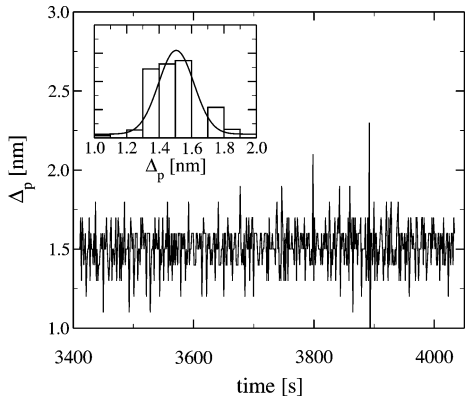


**Figure 5.** Noise of position sensor signal change while moving the lower surface 1.5 nm each step. The curved surfaces are not in contact. A histogram of the noise is shown in the inset. The accuracy of position measurement is given by the variance $\sigma_{p+t} = 2 \cdot \sqrt{\text{var}} = 0.22$ nm. The accuracy of stage movement can be obtained within the same experiment and is $\sigma_t = 0.13$ nm (data not shown).

0.5 nm/h. After a long period of thermal drifting and mechanical relaxation, we ended up with a setup providing very stable conditions for a couple of hours, which is needed for reliable single molecule experiments. Within this state we have characterized the mechanical measurement accuracies of our setup. As shown before (eqs 2 and 6), the accuracies of measuring the distance changes $\sigma_p$ (position sensor) and $\sigma_t$ (piezo translation stage) are dominating factors for the resulting accuracy of all mechanical experiments (change of applied force, change of film thickness).

To determine these uncertainties, the lower surface was moved by increasing the set point of the control loop of the piezo scanner in successive steps of 1.5 nm, while the surfaces were separated by an air gap. The changes of the signals at the position sensor as well as at the scanner sensor were recorded (Figure 5). From the obtained data $\Delta_t$ (piezo translation stage), the accuracy of stage movement $\sigma_t$ can be calculated as $\sigma_t = 2 \cdot \sqrt{\text{var}} = 0.13$ nm. While $\Delta_p$ is also accessible by reading the position sensor, its uncertainty is determined by the uncertainty of the sensor reading itself and the uncertainty in the adjusted change at the piezo translation stage $\Delta_t$. Thus, the signal $\Delta_p$ changes as a consequence of a change in $\Delta_t$. Therefore, the determined uncertainty of $\Delta_p$ is just a convolution of the corresponding (Gaussian) probability distributions for finding a certain $\Delta_p$ and $\Delta_t$. The resulting accuracy of the signal changes at the position sensor (which we therefore denote as $\sigma_{p+t}$), is $\sigma_{p+t} = 0.22$ nm and always larger than $\sigma_t$. The value of $\sigma_p$ itself is finally obtained from a deconvolution of Gaussians (widths $\sigma_{p+t}$ and $\sigma_t$, respectively):

$$\sigma_p = \sqrt{\sigma_{p+t}^2 - \sigma_t^2} = 0.18 \text{ nm}$$

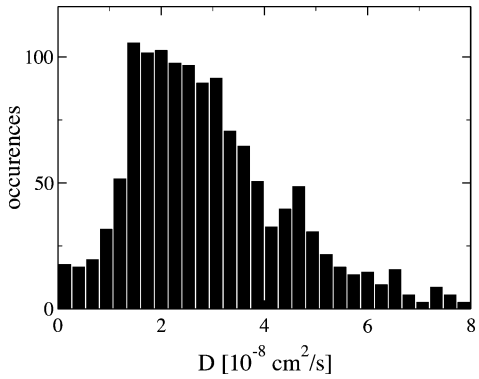


**Figure 6.** Distribution of single molecule diffusion constants measured for a liquid film in the gap of the SFA with a load of 1.5 N/m. The mean diffusion constant is $\langle D \rangle = 2.7 \times 10^{-8}$ cm$^2$/s. The comparison to the bulk value for TEHOS ($D_{bulk} = 3 \times 10^{-7}$ cm$^2$/s) shows a slow of about 1 order of magnitude.

Following this and using eq 2, we obtain $\sigma_F = 3$ $\mu$N as the measurement accuracy of detecting force changes. This corresponds to 0.04 mN/m if normalized by the radius of curvature of the surfaces. The accuracy of measuring liquid film thickness changes $\sigma_l$ is given by eq 6 and results in $\sigma_l = 0.83$ nm, which is, compared to other SFA experiments ($\sigma_l = 0.041$ nm[41]), not yet satisfactory. This huge difference is mainly attributed to the method of measuring the surface separation. Our setup can only detect changes in separation between two points of the SFA frame, whereas all setups with interferometrical thickness measurement directly detect the sample's thickness between the silvered substrates, which is obviously much more precise.

To demonstrate the single molecule tracking capabilities of our setup, we have placed a droplet of TEHOS doped with RhB between the MICA surfaces of the SFA. The lower surface was then raised against the upper one until a repulsion was detected, indicating a mechanical contact between the surfaces. It is important to adjust the apparatus in a way, that the region, where the surfaces are closest to each other, is directly beneath the microscope objective. This is achieved by moving the whole SFA part horizontally against the microscope part.

A coarse estimate of the film thickness in the observed sample region can be obtained by changing the optical focus from one to the other mica liquid interface, which can easily be identified due to a small number of attached dye molecules. If both surfaces are in focus at the same time, the film thickness should be below 300 nm, since otherwise characteristic defocusing patterns would be observed.[42] Following this adjustment procedure we applied different (high) loads. For each load we collected several thousand frames of diffusing molecules from the confined liquid layer. All molecules were tracked with our software. Each single molecule trajectory was used to obtain one diffusion coefficient. Thus, the measurement of several hundred molecules for each load allows to construct a distribution of diffusion coefficients for each load as for example depicted in Figure 6. Diffusion coefficients are found to be widely distributed (1 order of magnitude) with a mean value of about $\langle D \rangle = 2.7 \times 10^{-8}$ cm$^2$/s. The results at different loads further reveal no dependence of the mean diffusion constant on the applied load (Figure 7). The overall mean diffusion coefficient averaged over all measurements ($\langle D \rangle_{loads} = 3 \cdot 10^{-8}$ cm$^2$/s) is about 1 order of magnitude lower than the diffusion coefficient for bulk TEHOS ($D_{bulk} = 3 \times 10^{-7}$ cm$^2$/s). This slow down could be in principle because of two different effects. First of all, dye molecules with the above-mentioned mean diffusion coefficient travel a distance of 300 nm (the upper

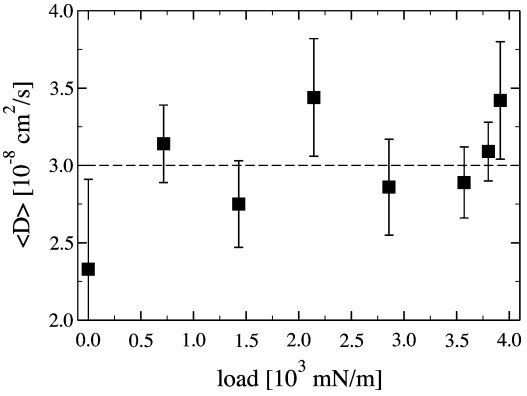


**Figure 7.** Mean single molecule diffusion constants at different applied loads. The graph reveals no clear dependence of the diffusion constant on the load. High loads have been chosen to ensure a thin liquid film (<300 nm), but actual film thickness is not known. The error bars indicate the width of the distribution as shown in Figure 6.

bound for the film thickness) in about 7.5 ms. Thus, they are expected to average over different spatial regions with different diffusion coefficients within the exposure time of 20 ms. On one side, these different spatial regions may just consist of an adsorption layer at the MICA surface and a free bulk layer between. Considering this type of model mixing adsorption and bulk diffusion, one can calculate the adsorption duration at the surface. Thus, a mean adsorption duration of 18 ms is required to obtain a mean diffusion coefficient of $\langle D \rangle_{\text{loads}} = 3 \cdot 10^{-8}$ cm$^2$/s. With respect to recent experiments,[29] the assumption of an adsorption at the MICA surface for such a long time seems to be unrealistic. According to references 29 and 43, the slowing of the diffusion is rather related to a change of the effective viscosity at the solid−liquid interface due to solid−liquid interactions. Therefore, an interfacial region exists in which molecules are trapped for a certain time (on the time scale of several milliseconds) without being immobilized. Following this idea, the obtained mean diffusion coefficient is necessarily independent from the applied load, if the overall thickness of the confined liquid is notably larger than twice the size of this interfacial region. Both regions of liquid close to the solid surfaces, where all detected dye molecules have been located, are obviously unaffected by thickness changes in the middle part (more distant from the surfaces) of the liquid. To induce a load dependence of the diffusion coefficient one has to squeeze the film to a thickness below twice the size of this interfacial region, which corresponds to the observation of density oscillations due to liquid layering starting at about 10 nm film thickness.[7] This film thickness region was, however, not reached with the present loads.

## 6. Summary

We have presented for the first time a setup which allows the tracking of single fluorescent molecules in a surface forces apparatus. The combination of both, the surface forces technique and the tracking of single fluorescent dye molecules using a widefield video microscope, promises access to molecular motion in confined liquid films and, therefore, allows new insights into well-established experimental results.

We have presented the mechanical performance of our setup, which is sufficient to detect changes of the liquid film thickness on a nanometer scale and to detect changes of the applied normal force with an accuracy of some $10^{-6}$ N. Highly specialized SFA setups are much better with respect to these parameters, but the presented setup allows a range of improvements to the current performance. With mechanical and thermal insulation the setup provides stable conditions for several hours to carry out optical experiments. Finally, we have shown that the setup is able to detect single dye molecules in confined liquid films of a few 100 nm film thickness with a time resolution of 20 ms and a localization accuracy of the dye molecules of about 50 nm. Despite a number of still unresolved technical problems we believe that this type of experiments will shine new light on the molecular details of liquid structure and dynamics under confinement and shear. Indeed, first preliminary experiments on single molecule detection in sheared liquids have been successful.

**Acknowledgment.** This project was funded by Volkswagen-Stiftung under Grant No. I/78834.

## References and Notes

(1) Tabor, D.; Winterton, R. H. S. *Proc. R. Soc. London A* **1969**, *312*, 435.
(2) Israelachvili, J. N.; Adams, G. E. *J. Chem. Soc., Faraday Trans.* **1978**, *74*, 975.
(3) Belouschek, P.; Meier, S. *Prog. Colloid Polymer Sci.* **1986**, *72*, 43.
(4) Götze, T.; Sonntag, H. *Colloid Surf.* **1987**, *25*, 77.
(5) Tonck, A.; Georges, J. M.; Loubet, J. L. *J. Colloid Interface Sci.* **1988**, *126*, 150.
(6) Parker, J. L.; Christenson, H. K.; Ninham, B. W. *Rev. Sci. Instrum.* **1989**, *60*, 3135.
(7) Horn, R. G.; Israelachvili, J. N. *J. Chem. Phys.* **1981**, *75*, 3.
(8) Chan, D. Y. C.; Horn, R. G. *J. Chem. Phys.* **1985**, *83*, 5311.
(9) Klein, J.; Kumacheva, E. *Science* **1995**, *269*, 816.
(10) Demirel, A. L.; Granick, S. *Phys. Rev. Lett.* **1996**, *77*, 2261.
(11) Drummond, C.; Israelachvili, J. N. *Phys. Rev E* **2001**, *63*, 041506.
(12) Gourdon, D.; Israelachvili, J. N. *Phys. Rev. E* **2003**, *68*, 021602.
(13) Raviv, U.; Giasson, S.; Kampf, N.; Gohy, J.-F.; Jerome, R.; Klein, J. *Nature* **2003**, *425*, 163.
(14) Tadmor, R.; Janik, J.; Klein, J. *Phys. Rev. Lett.* **2003**, *91*, 115503.
(15) Mugele, F.; Salmeron, M. *Phys. Rev. Lett.* **2000**, *84*, 5796.
(16) Mugele, F.; Salmeron, M. *J. Chem. Phys.* **2001**, *114*, 1831.
(17) Becker, T.; Mugele, F. *J. Phys.: Condens. Matter* **2003**, *15*, 321.
(18) Mukhopadhyay, A.; Zhao, J.; Bae, S. C.; Granick, S. *Rev. Sci. Instrum.* **2003**, *74*, 6.
(19) Mukhopadhyay, A.; Zhao, J.; Bae, S. C.; Granick, S. *Phys. Rev. Lett.* **2004**, *93*, 236105.
(20) Deschenes, L. A.; Bout, D. A. V. *Nature* **2001**, *292*, 255.
(21) Schob, A.; Cichos, F.; Schuster, J.; v. Borzcyskowski, C. *Eur. Polym. J.* **2004**, *40*, 1019.
(22) Schütz, G. J.; Schindler, H.; Schmidt, T. *Biophys. J.* **1997**, *73*, 1073.
(23) Schütz, G. J.; Kada, G.; Pastushenko, V. P.; Schindler, H. *EMBO J.* **2000**, *19*, 892.
(24) Ishii, Y.; Yanagida, T. *Single Molecules* **2000**, *1*, 5.
(25) Seebacher, C.; Hellriegel, C.; Deeg, F.-W.; Bräuchle, C.; Altmeier, S.; Behrens, P.; Müllen, K. *J. Phys. Chem. B* **2002**, *106*, 5591.
(26) Seebacher, C.; Hellriegel, C.; Bräuchle, C.; Ganschow, M.; Wöhrle, D. *J. Phys. Chem. B* **2003**, *107*, 5445.
(27) Hellriegel, C.; Kirstein, J.; Bräuchle, C.; Latour, V.; Pigot, T.; Olivier, R.; Lacombe, S.; Brown, R.; Guieu, V.; Payrastre, C.; Izquierdo, A.; Mocho, P. *J. Phys. Chem. B* **2004**, *108*, 14699.
(28) Schuster, J.; Cichos, F.; v. Borzcyskowski, C. *Eur. Polym. J.* **2004**, *40*, 993.
(29) Schuster, J.; Cichos, F.; von Borczyskowski, C. *Eur. Phys. J. E* **2003**, *12*, 75.
(30) Heuberger, M. *Rev. Sci. Intrum.* **2001**, *72*, 1700.
(31) Parker, J. L. *Langmuir* **1992**, *8*, 551.
(32) Frantz, P.; Agrait, N.; Salmeron, M. *Langmuir* **1996**, *12*, 3289.
(33) Frantz, P.; Artsyukhovich, A.; Carpick, R. W.; Salmeron, M. *Langmuir* **1997**, *13*, 5957.
(34) Restagno, F.; Crassous, J.; Charlaix, E.; Monchanin, M. *Meas. Sci Technol.* **2001**, *12*, 16.
(35) Restagno, F.; Crassous, J.; Charlaix, E.; Cottin-Bizonne, C.; Monchanin, M. *Rev. Sci. Instrum.* **2002**, *72*, 6.
(36) Heslot, F.; Fraysse, N.; Cazabat, A. M. *Nature* **1989**, *338*, 640.
(37) Frantz, P.; Salmeron, M. *Trib. Lett.* **1998**, *5*, 151.
(38) Horn, R. G.; Israelachvili, J. N.; Pribac, F. J. *Colloid Interface Sci.* **1987**, *115*, 480.
(39) Göldner, H.; Witt, D. *Technische Mechanik I, Statik und Festigkeitslehre*; FachbuchverlagLeipzig-Köln: Leipzig, 1993.
(40) Saxton, M. J. *BioPhys. J.* **1997**, *72*, 1744.
(41) Zäch, M.; Vanicek, J.; Heuberger, M. *Rev. Sci. Intrum.* **2003**, *74*, 260.
(42) Böhmer, M.; Enderlein, J. *J. Opt. Soc. Am. B* **2003**, *20*, 554.
(43) Becker, T.; Mugele, F. *Phys. Rev. Lett.* **2003**, *91*, 166104.